Dynamics of contracting filaments

Christopher R. Anthony,* Pritish M. Kamat, Michael T. Harris, and Osman A. Basaran†
Davidson School of Chemical Engineering, Purdue University, 480 Stadium Mall Drive, West Lafayette, Indiana 47907, USA

(Received 4 February 2019; published 3 September 2019)

The contraction of liquid filaments plays a central role in applications as diverse as inkjet printing and atomization where the formation of monosized primary drops is desirable, but that of smaller satellite droplets is typically undesirable. In order to avoid polydisperse drop sizes and/or minimize the deleterious consequences of satellite droplet production, contracting or retracting filaments formed during drop pinch-off and liquid atomization should either contract to spheres without further breakup or break into equally sized drops. Therefore, given the importance of understanding the fate of contracting filaments, high-accuracy numerical simulations are used to analyze the retraction of Newtonian liquid filaments in a passive outer fluid. Previously, Notz and Basaran [Notz and Basaran, J. Fluid Mech. **512**, 223 (2004)] provided a comprehensive description of the dynamics of low-viscosity filaments and subsequent studies have helped to advance our understanding of the response of moderate- to high-viscosity filaments. However, as it is shown here, combining the findings of all of these separate works does not provide a complete picture of the rich physics of filament contraction. In this work, a comprehensive approach is adopted to further refine and expand upon earlier works to provide a complete phase diagram of filament retraction dynamics by considering the entire possible range of fluid properties and initial aspect ratios for filaments undergoing contraction. In doing so, a different mode of breakup, herein referred to as capillary wave breakup, is discovered and shown to be the dominant mode of pinch-off for moderately viscous filaments. The mechanism for the breakup of filaments of moderately viscous fluids is detailed along with a thorough investigation of the already established modes of breakup for nearly inviscid and highly viscous filaments.

DOI: 10.1103/PhysRevFluids.4.093601

I. INTRODUCTION

Many industrial applications require the production of large numbers of drops of identical size, primary drops, while minimizing or avoiding the production of smaller satellite droplets, or fines, that are almost always undesirable [1]. Such applications arise in fields as diverse as inkjet printing using both drop-on-demand (DOD) and continuous inkjet techniques [2–6], atomization- or spray-based coating, painting, and agricultural crop protection operations [7–9], microarraying of DNA, and printing of cells as well as other biological materials in life sciences [10,11], printing of drugs on edible substrates for personalized medicine [12], and drop-by-drop additive manufacturing and three-dimensional printing in materials science and electronics [13–15]. A common feature of drop formation operations is the occurrence of long, slender liquid filaments which, due to surface tension, contract and undergo further breakup. For example, when drops are emitted from

*anthonc@purdue.edu
†obasaran@purdue.edu

DOD inkjet nozzles, they resemble long, slender filaments [16]. In both dripping [17] and jetting [18], larger drops are connected to the nozzle or each other by long, slender filaments prior to breakup. In atomization or spraying, long, slender filaments are generated from the disintegration of liquid jets [19,20] and sheets [21,22], which then contract to give rise to spray drops. In order to avoid polydisperse drop sizes and/or minimize the formation of satellites, contracting or retracting filaments should either contract to spheres without further breakup or break into equal-sized drops. Therefore, improving the understanding of the fate of contracting liquid filaments is key to developing fundamental insights into the fluid dynamics of drop formation processes and is the primary goal of this paper.

The dynamics of contracting filaments did not receive much attention until the experimental study of Stone *et al.* [23], in which the filaments were stretched by an imposed flow in the outer fluid and subsequently allowed to relax. While the study of Stone *et al.* and many others that were motivated by it (see, e.g., [24]) entailed the recoil of liquid filaments that were surrounded by another dynamically active liquid and where both liquids were undergoing creeping or Stokes flow at zero Reynolds number, the problem under study in this paper entails filament recoil in a dynamically passive ambient fluid, e.g., air, at finite Reynolds number. Despite this important difference, the two problems nevertheless have certain features in common. Stone *et al.* observed that as a filament contracts, it may successively pinch off drops from its two ends by a breakup mechanism that is now commonly referred to as end pinching. It was also observed that even in cases where the Rayleigh-Plateau instability [25–27] would be expected to develop and manifest itself along the surface of sufficiently long filaments and which would subsequently result in the filament to break up into many drops, this instability did not occur. The latter observation suggested that the timescale for the Rayleigh-Plateau instability to grow is much larger than the timescale for the filament to fully contract even for long filaments.

Motivated in part by the aforementioned findings by Stone *et al.* [23], Schulkes [28] numerically studied, using a Galerkin finite-element-method (GFEM) -based algorithm, the contraction of free filaments of Newtonian liquids undergoing incompressible flow in the absence of an external medium, or when that medium is a passive fluid that simply exerts a constant pressure on the filament, at finite Reynolds number. In Schulkes's study and in many others that followed it, the initial filament shape consisted of a long cylinder with hemispherical caps at both ends. However, owing to computational challenges, Schulkes was only able to simulate the onset of end pinching: The meshing algorithm that his code used broke down as the filament recoiled and he was unable to simulate the extreme interfacial deformations that arose as the filament tended toward pinch-off. Among the many insightful contributions reported in this pioneering study, it was shown that the dynamics of filament contraction can be completely described by two dimensionless groups: the Ohnesorge number Oh, which measures the relative importance of viscous force to the square root of the product of inertial and capillary (surface tension) forces, and the dimensionless initial aspect ratio L_0. Further progress on the problem was made by Notz and Basaran [29], who employed an improved meshing scheme with a different GFEM-based algorithm which allowed them to accurately model the entire contraction and breakup process. A key finding of their study was the existence of both a critical Ohnesorge number Oh_c above which a filament will never undergo breakup and a critical initial aspect ratio L_c, for a given value of Oh, below which a filament will fully contract without breakup. Notz and Basaran constructed a phase diagram for contracting filaments and also reported values of L_c for a range of Oh. However, owing to the fact that computation time grew linearly with the initial aspect ratio, Notz and Basaran did not consider the fates of filaments of extraordinarily large initial aspect ratios.

Filament contraction in a passive ambient fluid has been receiving increasing attention in recent years. Castrejón-Pita *et al.* [30] carried out experiments on filament contraction in which they considered a wider range of initial aspect ratios and Ohnesorge numbers than which had heretofore been studied. These authors showed that experimental results appeared to agree well with simulations and theory for $\mathrm{Oh} < 0.05$, while there was discrepancy between results for more viscous and longer filaments. However, it was unclear if the discrepancy was due to inaccuracy in numerical

simulations or inconsistency between the simulations and experimental conditions. Subsequently, Driessen *et al.* [31] solved a set of spatially one-dimensional transient partial differential equations based on the slender-jet approximation [1,32,33] and showed that long viscous filaments may indeed succumb to a Rayleigh-Plateau instability. However, in all of the simulations carried out by these authors, a perturbation was applied to initiate the instability rather than allowing one to arise naturally during the contraction of the filament. Additionally, a relation predicting the value of L_c as a function of Oh was estimated from a comparison of the time for filament contraction to the growth rate of the instability that would cause the breakup of the filament. It is noteworthy that this relation between L_c and Oh was also dependent on a third parameter, the value of the initial perturbation applied to the contracting filament. However, by tuning the value of this perturbation, Driessen *et al.* found reasonable agreement between their predictions and experiments [30] for $\mathrm{Oh} > 0.1$, a finding that suggested that experiments were perhaps also vulnerable to perturbations imposed during the creation of these filaments. Thus, while it appeared at this point that there was reasonably good agreement between experiments on the one hand and simulations and theory on the other hand for both low-viscosity (Oh) filaments for which breakup occurs through end pinching and for high-viscosity (Oh) filaments for which breakup occurs via a Rayleigh-Plateau-type instability, uncertainty still remained with respect to the mechanism(s) of filament breakup for intermediate viscosities (Oh). More recently, Hoepffner and Paré [34] investigated this intermediate range through both experiments and simulations. These authors thereby showed that filaments of intermediate Oh can escape from end pinching as they recoil, which can mitigate or greatly delay breakup due to end pinching. This escape phenomenon can occur multiple times, and the escape from and/or approach to end pinching results in a discontinuous variation of breakup time and the critical initial aspect ratio with Oh. These results suggested that a phase diagram of L_c versus Oh should have a steplike appearance in the intermediate range of Ohnesorge numbers.

It is clear that one of the most sought after measures in quantifying filament contraction is the critical value of the initial aspect ratio L_c. However, past studies have been inconsistent as to what is exactly meant by L_c. Some studies define L_c such that filaments of initial aspect ratio $L_0 < L_c$ will always fully contract to a sphere sans breakup. In this paper, this critical value of the initial aspect ratio will be denoted by $L_{c,1}$. Others define L_c such that filaments of initial aspect ratio $L_0 > L_c$ will always break before full contraction. Here this critical value of the initial aspect ratio will be denoted by $L_{c,2}$. While either definition is appropriate in its own right, confusion can result when comparing values of L_c obtained from different studies if it is implicitly assumed that $L_{c,1} \equiv L_{c,2}$. Although papers published to date provide no evidence to the contrary, it is nevertheless prudent to investigate whether this assumption is universally valid. In this work, the validity of this assumption is also tested.

The goal of this paper is to analyze by means of high-accuracy simulation the contraction of free filaments of incompressible Newtonian fluids that are surrounded by a passive ambient fluid for a wider range of both the initial aspect ratios and fluid properties than has been done to date and to construct a phase diagram summarizing the fates of retracting filaments over the entire parameter space described by these variables. Section II provides the mathematical formulation of the problem solved and summarizes the numerical method used to carry out the simulations. Section III begins by presenting results of a comprehensive investigation of the dynamics of filaments of intermediate viscosity (Oh) which has been the least well studied portion of the parameter space. Here a different class of breakup modes is also uncovered and an in depth analysis is carried out to decipher the mechanisms behind them. Section IV presents the results of filament contraction in the inviscid regime for filaments of slightly viscous or nearly inviscid (small Oh) fluids. Here, in addition to validating the predictions made with the algorithm used in this paper, additional aspects of the dynamics are also highlighted. Section V details the dynamics of filament contraction for highly viscous (large Oh) filaments. In this section, in contrast to previous studies in which a perturbation is imposed to cause filament breakup, it is shown that perturbations arise naturally during filament contraction. The article concludes with a summary of results in the form of a phase diagram that delineates regions of the parameter space where filaments contract without undergoing breakup

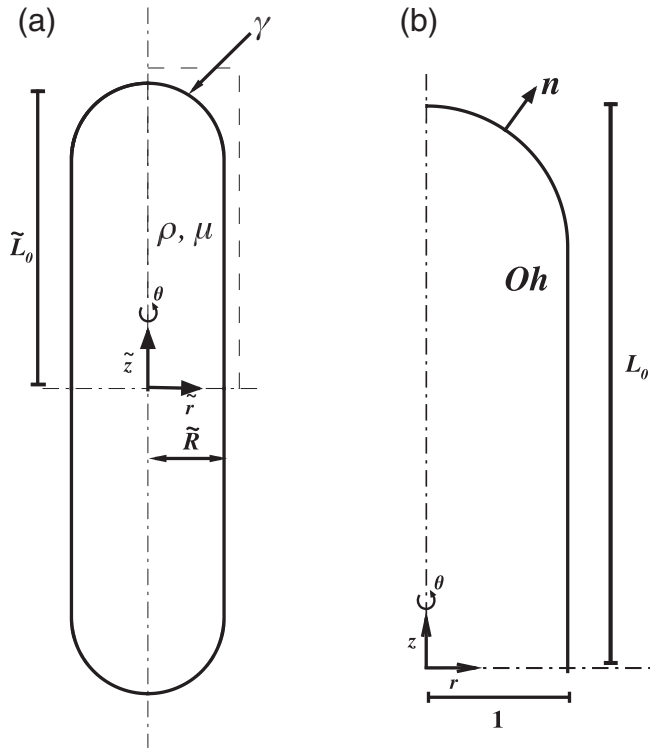

FIG. 1. (a) Definition sketch showing the initial shape of a Newtonian filament, and the key variables and the coordinate system used in dimensional form. (b) Sketch showing the problem domain that consists of a single quadrant of the (r, z) plane at the initial instant, the governing dimensionless groups Oh and L_0, and the coordinate system used in dimensionless form.

from ones where breakup occurs along with clear identification of the various mechanisms that cause breakup in the different regions where pinch-off occurs.

II. MATHEMATICAL FORMULATION AND NUMERICAL METHOD

A. Mathematical formulation

The system is a free liquid filament of an incompressible Newtonian fluid of constant density ρ and constant viscosity μ that is surrounded by a dynamically passive gas that exerts a constant pressure on the filament. The surface tension of the interface between the two fluids γ is spatially uniform and constant in time. Initially at time $\tilde{t} = 0$, the fluid within the filament is quiescent, viz., $\tilde{\mathbf{v}} = \mathbf{0}$, where $\tilde{\mathbf{v}}$ is the velocity, and the filament's shape is that of a long cylinder of radius $\tilde{R}$ that is terminated at both ends by identical hemispherical caps of radii $\tilde{R}$, as shown in Fig. 1. The initial shape of the filament is axisymmetric and its initial half length, measured along the axis of symmetry from either tip to the plane of symmetry, is given by $\tilde{L}_0$. Therefore, the filament's aspect ratio initially equals $\tilde{L}_0/\tilde{R}$. In what follows, it turns out to be convenient to use a cylindrical coordinate system $(\tilde{r}, \theta, \tilde{z})$, where $\tilde{r}$, θ, and $\tilde{z}$ stand for the radial coordinate, the angle measured around the axis of symmetry, and the axial coordinate, with its origin at the center of the filament or the intersection of the axis of symmetry $\tilde{r} = 0$ and the plane of symmetry $\tilde{z} = 0$.

The problem is nondimensionalized by using $\tilde{R}$ as characteristic length l_c, the inertial-capillary time $\sqrt{\rho\tilde{R}^3/\gamma}$ as characteristic time t_c, the ratio of the latter two scales as characteristic velocity $v_c = l_c/t_c$, and the capillary pressure $\gamma/\tilde{R}$ as characteristic pressure or stress. As a result, the

problem is governed by just two dimensionless groups: the Ohnesorge number $\mathrm{Oh} = \mu/\sqrt{\rho\tilde{R}\gamma}$ and the dimensionless initial aspect ratio $L_0 = \tilde{L}_0/\tilde{R}$. In what follows, variables without tildes over them denote the dimensionless counterparts of those with tildes, e.g., whereas $\tilde{r}$ is dimensional, $r \equiv \tilde{r}/\tilde{R}$ stands for the dimensionless radial coordinate.

The dynamics in the region $\Omega(t)$ occupied by the fluid contained within the filament is governed by the axisymmetric form of the Navier-Stokes and continuity equations which in dimensionless form are given by

$$\frac{\partial \mathbf{v}}{\partial t} + (\mathbf{v}\cdot\nabla)\mathbf{v} = \nabla\cdot\mathbf{T}, \tag{1}$$

$$\nabla\cdot\mathbf{v} = 0. \tag{2}$$

Here $\mathbf{v} \equiv \tilde{\mathbf{v}}/v_c$ is the dimensionless fluid velocity, $t \equiv \tilde{t}/t_c$ is the dimensionless time, and $\nabla \equiv \tilde{R}\tilde{\nabla}$ is the dimensionless gradient operator. The dimensionless stress tensor for the Newtonian fluid is given as $\mathbf{T} \equiv \tilde{\mathbf{T}}/p_c = -p\mathbf{I} + \mathrm{Oh}[\nabla\mathbf{v} + (\nabla\mathbf{v})^T]$, with $p \equiv \tilde{p}/p_c$ defining the dimensionless pressure. The pressure in the dynamically passive fluid exterior to the filament is taken to be the datum level of pressure.

The domain $\Omega(t)$ over which Eqs. (1) and (2) are solved is enclosed by the free surface of the contracting filament, $S(t)$, which is unknown *a priori*. Due to axial symmetry and reflective symmetry about the midplane of the filament, the domain over which the governing equations are solved is reduced to one quadrant of the (r, z) plane that is bounded by the free surface, which is a curve whose unknown shape is to be determined as part of the solution, the symmetry axis $r = 0$, and the plane (line) of symmetry $z = 0$. Symmetry boundary conditions are applied along the latter two boundaries. Along the free surface $S(t)$, the kinematic and traction boundary conditions are applied to determine the unknown shape of the interface and account for the discontinuity in stress due to surface tension:

$$\mathbf{n}\cdot(\mathbf{v} - \mathbf{v}_s) = 0, \tag{3}$$

$$\mathbf{n}\cdot\mathbf{T} = -2\mathcal{H}\mathbf{n}. \tag{4}$$

Here $2\mathcal{H} = 2\tilde{\mathcal{H}}\tilde{R}$ is twice the dimensionless local mean curvature of the interface, $\mathbf{n}$ is the outward pointing unit normal to it, and $\mathbf{v}_s = \tilde{\mathbf{v}}_s/v_c$ is the dimensionless velocity of points along the free surface $S(t)$.

B. Numerical method

The transient system of partial differential equations, boundary conditions, and initial conditions given in the preceding section is solved using a fully implicit, arbitrary Lagrangian-Eulerian method of lines algorithm in which the GFEM is employed for spatial discretization [35] and an adaptive, implicit finite-difference method is deployed for time integration [36]. In order to capture the large deformations and breakup of the fluid interface that may occur during filament contraction, the elliptic mesh generation method that was developed by Christoloudou and Scriven [37] for studying thin-film coating flows and which was later adapted for studying free surface flows of Newtonian and complex fluids involving breakup and coalescence [29,38–41] is employed to discretize the domain and determine the axial and radial coordinates of each grid point as the mesh deforms in time in response to the motion of the free surface. The velocity and pressure unknowns are solved in a mixed interpolation scheme where the velocity unknowns are represented in terms of biquadratic basis functions while the pressure unknowns are represented by means of bilinear basis functions [42]. Also, in the present algorithm, the unknown coordinates of the grid or mesh points are represented by biquadratic basis functions. With the aforementioned spatial and temporal discretizations, the computational problem is reduced to a system of nonlinear algebraic equations which is solved via

a multidimensional Newton's method. The resulting linear system is solved at each iteration by a multifrontal algorithm which was derived from the frontal algorithm developed by Hood [43].

The numerical method used here, with the exception of the multifrontal algorithm, is virtually the same as that used by Notz and Basaran [29] in their study of filament contraction. For a more in depth description of the numerical method used, the reader is referred to their work and that of Anthony [44]. In this paper, breakup or pinch-off is said to have occurred when the minimum radius of the filament falls below 10^{-3}. Before commencing a detailed discussion of the dynamics of contracting filaments, the reader is referred to the Appendix, in which the results of a number of code validation and mesh refinement studies are presented.

III. INTERMEDIATE REGIME ($0.002 < \mathrm{Oh} < 0.1$)

Filaments of very small initial aspect ratio L_0 do not break, but ones of sufficiently large L_0 may. In classifying modes of breakup that are observed during filament contraction as the value of L_0 is systematically increased at a fixed value of Oh, it proves convenient to sort the breakup modes into two main categories: (a) breakup modes for filaments of indefinitely long lengths, which are henceforward called final breakup modes, and (b) breakup modes for filaments of intermediate lengths, which are henceforth referred to as intermediate breakup modes. Here we define a final breakup mode as that which will always occur if the filament's initial aspect ratio is larger than some critical value and, when breakup does occur, it will always occur in virtually the same amount of time regardless of the value of the initial aspect ratio. Conversely, intermediate breakup modes are those that do not follow the previous criteria. Specifically, intermediate breakup modes occur over only a certain range of L_0, and the time at which breakup occurs is not constant and in fact varies with L_0. Given these definitions, as the initial filament aspect ratio is increased from a small value, the smallest value of L_0 at which an intermediate breakup mode occurs corresponds to $L_{c,1}$ while the smallest value of L_0 beyond which all filaments of initial aspect ratios exceeding that value succumb to the final breakup mode correspond to $L_{c,2}$. If an intermediate breakup mode does occur, $L_{c,2} > L_{c,1}$ and typically $L_{c,2} \gg L_{c,1}$ (discussed below). If, however, an intermediate breakup mode does not arise, then of course there is only one critical initial aspect ratio and $L_{c,1} \equiv L_{c,2}$.

Prior to this paper and as has already been discussed in the Introduction, a considerable amount of work has been done on filaments of either large or small Ohnesorge numbers, but much less effort has been expended on filaments of intermediate Oh. Thus, it is imperative to summarize in greater detail findings reported in earlier studies in light of the definitions of final and intermediate breakup modes and the two different values of the critical initial aspect ratio, $L_{c,1}$ and $L_{c,2}$, introduced in the preceding paragraph, and to differentiate the approach that is taken in this work in carrying out simulations compared to earlier studies. By now, it has been well established that filaments of small Oh and sufficiently large L_0 will immediately succumb to end pinching [23,28–30]. However, Hoepffner and Paré [34] have shown that for $0.002 < \mathrm{Oh} < 0.1$, there will be one or more escape events from end pinching before the filament ultimately breaks. In an escape event, the thinning neck that forms between the receding blob and the main cylindrical body of the filament suddenly reopens, thereby greatly increasing the time until breakup. By simulating the dynamics of semi-infinite filaments, these authors concluded that the critical value of the initial aspect ratio was equal to the recoiling length at a given value Oh. These simulations, which yielded the critical initial aspect ratio for both nearly inviscid filaments and ones of intermediate values of Oh, were then combined with the results of the study of long viscous filaments by Driessen *et al.* [31] to construct a phase diagram of the critical initial aspect ratio ($L_{c,2}$) over the entire range of Oh. However, as these simulations were of semi-infinite filaments, any interactions across the midplane of the filament ($z = 0$) were assumed not to have any significant effect in either hindering or promoting breakup. Rather than making this assumption, we have carried out a thorough study of the effect of the initial aspect ratio by varying it from nearly unity until it just exceeded $L_{c,2}$ in order to test the assumption of no or negligible interactions across the midplane of filaments. In what follows, the

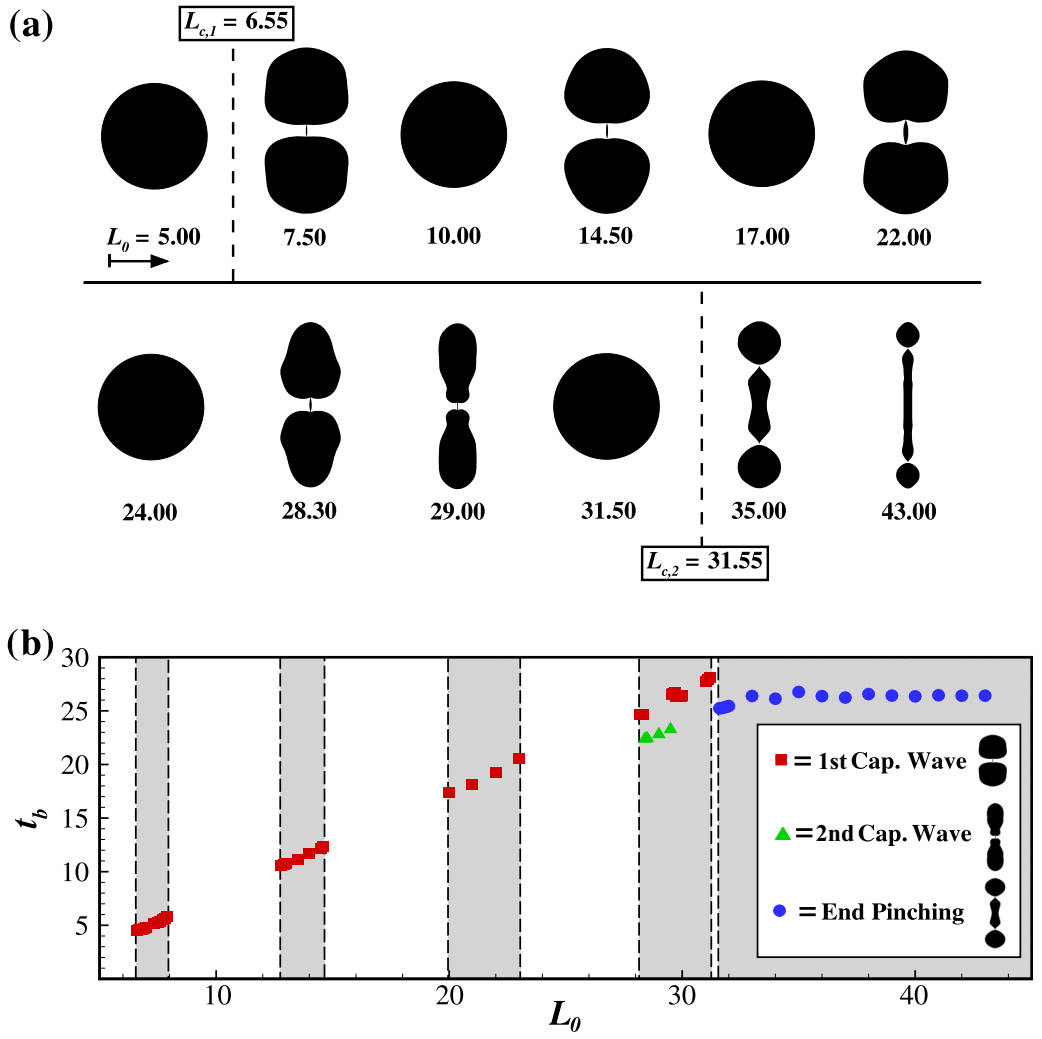

FIG. 2. Breakup shapes and breakup times of filaments that undergo pinch-off or final shapes of filaments that do not break up when Oh = 0.03. (a) Variation of shapes at breakup (not to scale) with L_0 showing a pattern of breakup and nonbreakup. If there is no breakup for a particular value of L_0, the spherical shape that corresponds to that value of L_0 indicates that the filament tends to a quiescent fluid sphere at large times. All filaments of initial aspect ratios $L_0 \geqslant L_{c,2}$ break up by end pinching. (b) Variation of breakup time t_b with L_0. Filaments whose initial aspect ratios L_0 lie in ranges shaded in gray are those that undergo breakup at time t_b as indicated in the figure. Filaments whose initial aspect ratios L_0 lie in ranges shaded in white, however, do not break and tend to spheres at large times. When filament contraction leads to breakup, the type of breakup that results is identified by using different symbols and a typical shape is shown for each breakup mode in the legend. Squares and triangles are used to denote cases of first and second capillary wave breakup (where "Cap." is the abbreviation for capillary), respectively, whereas circles are used to identify cases where breakup occurs by end pinching.

results of a detailed computational study are presented for filaments of Oh = 0.03, which is a case that is representative of the dynamics that is observed in the intermediate regime.

Figure 2(a) shows the profiles at breakup, or breakup shapes, of contracting filaments over a large range of values of the initial aspect ratio when Oh = 0.03. It should be noted that for

filaments of small L_0, the filaments fully contract and, upon complete retraction, undergo complex oscillations. However, at this value of Oh, the oscillations, although often nonlinear and of large amplitude, are damped by viscosity and breakup does not occur (cf. [45]). As L_0 is systematically increased, breakup is first shown for a filament of $L_0 = 7.5$. Here the breakup shape is that of two large blobs that are connected by a small bridge of fluid, as shown in Fig. 2(a). Based on the current understanding of filament breakup, one might suspect that breakup has occurred by the well known end pinching mechanism for this filament that is just long enough such that its two ends have had enough time to pinch off. However, as filaments of increasingly larger initial aspect ratios are considered, this breakup mode does not persist and, indeed, a filament of $L_0 = 10$ does not even break upon recoiling. Remarkably, the mode of breakup that was first observed around $L_0 = 7.5$ also occurs for filaments in a small range of L_0 surrounding the values of 14.5, 22, and 28.3 and for which the breakup shapes are quite similar. For values of L_0 that lie between the aforementioned values where breakup occurs, there exist finite ranges of L_0 where filaments fully recoil to spheres without undergoing breakup. This pattern of breakup and nonbreakup repeats as L_0 increases. Although the breakup shapes remain qualitatively similar in that they always have the appearance of two blobs that are connected by a small bridge, the blobs become less spherical and more elongated as L_0 increases, as shown in Fig. 2(a), and in particular when $L_0 = 29$. This pattern of breakup and nonbreakup finally ends when the initial aspect ratio $L_0 \approx 31.5$ and beyond which recoiling filaments break by true end pinching. Plainly, since $L_{c,1} = 6.55$ and $L_{c,2} = 31.55$, there is not a single value of the critical initial aspect ratio at this Oh and a clear discrepancy exists between the two definitions used by different previous investigators to describe the critical initial aspect ratio. The mode of breakup that is observed over the range of L_0 lying between 6.55 and 31.55 is henceforward referred to as capillary wave breakup. The reason behind this name will become clear after delving into the detailed analysis that is presented below of the mechanism underlying this mode of breakup.

Figure 2(b) shows the variation of breakup time t_b with initial aspect ratio L_0 and elucidates a key difference between capillary wave breakup and end pinching: Whereas t_b increases with L_0 in capillary wave breakup, it takes virtually the same amount of time for breakup by end pinching regardless of the value of L_0. Moreover, drops of roughly constant volume are observed to pinch off from the two ends of a filament undergoing end pinching. The latter observation accords with intuition since the recoil time, and hence length, is virtually the same regardless of the value of L_0, thereby resulting in the accumulation of nearly an equal amount of fluid in the two globular ends that ultimately pinch off from the recoiling filament. By contrast, in capillary wave breakup, whereas the sizes of the droplets that are shed are not the same, the profiles at breakup are virtually the same as L_0 varies. Since in all instances of capillary wave breakup the profile at breakup or the breakup shape is always two nearly spherical drops that are connected by a small bridge and because nearly all of the fluid in the filament ends up being partitioned equally in the two end drops at pinch-off, the total volume, and hence the volume of the two drops at the two ends, also increases as L_0 increases. It should be noted that while the breakup shapes appear to be of the same size in Fig. 2(a), they only are so because they are not drawn to scale in order to allow them to be presented in a single figure. Armed with the knowledge that breakup always occurs just ahead of the receding ends and also that breakup only occurs just prior to full contraction, it proves instructive to investigate the behavior of the first local minima of the free surface just ahead of the receding blob, denoted by R_b, whose temporal variation and definition are shown in Fig. 3.

Figure 3(a) shows the evolution in time t of R_b for all of the filaments of Fig. 2(a) that underwent capillary wave breakup with the exception of the filament of $L_0 = 29$. It can be seen that the time evolution of R_b is virtually independent of L_0 throughout the entire period of recoil and all of the results collapse for the most part onto a single master curve which depicts the variation of R_b with t of a very long filament with $L_0 \gg L_{c,2}$ (this is the case of $L_0 = 74.25$, a filament that is so long that it breaks by end pinching). According to the results shown in Fig. 3(a), once filaments of $L_0 < L_{c,2}$ are near full contraction, the two ends begin to interact with each other across the symmetry plane $z = 0$ and culminate in the filament catastrophically tending toward pinch-off. While this

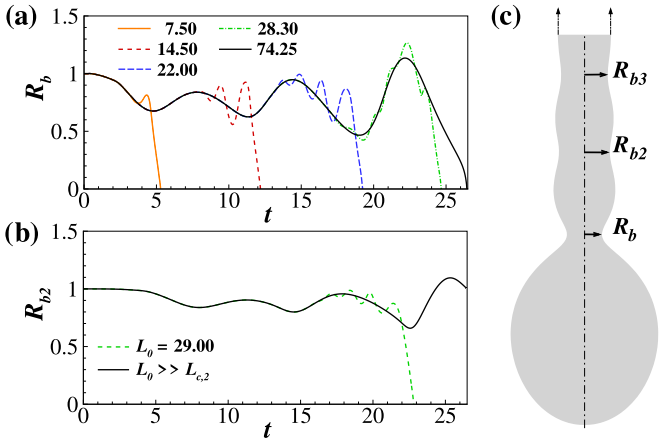

FIG. 3. Time evolution of minima in the filament radius when Oh = 0.03 and definition sketch showing different minima. (a) Evolution in time t of the radius R_b at the first minimum for filaments of $L_0 = 7.5$, 14.5, 22, and 28.3 that undergo first capillary wave breakup. Also shown is the response of a long filament of $L_0 = 74.25$ that breaks by end pinching. (b) Time evolution of R_{b2}, filament radius at the second minimum, for the single case of $L_0 = 29$ that undergoes second capillary wave breakup. Also shown is the response of a long filament of initial aspect ratio that is much larger than $L_{c,2}$. (c) Sketch that shows the first, second, and third minima R_b, R_{b2}, and R_{b3}, respectively.

interaction-induced destabilization arises in all cases, it has the greatest impact when the time for a filament of $L_0 < L_{c,2}$ to fully contract corresponds to the time at which the R_b versus t for the master curve is at one of its minima. Indeed, the only filaments that actually achieve pinch-off via the capillary wave breakup mechanism do so at times corresponding to these minima in R_b.

A cursory examination of the dynamics of the filament of $L_0 = 29$ shows that it does not strictly follow the pattern of response described in the preceding paragraph. In fact, the breakup location of this filament is not at R_b but instead occurs where a second minimum in the thread's radius, R_{b2}, from the receding end is located. If the time variation of R_{b2} in lieu of R_b is monitored, Fig. 3(b) shows that a dynamical response that is similar to that exhibited by R_b in the previous cases is observed in that the breakup time corresponds to a minimum in time for R_{b2} rather than R_b. This finding strongly suggests that an identical mechanism for disrupting the filament is at work here as in the other cases described in the preceding paragraph albeit at a different location. Thus, we further subclassify the modes of breakup described in the preceding paragraph and the current one as the first and second capillary wave breakup modes.

While we now know the conditions under which the capillary wave breakup mode will occur, the exact mechanism behind it is still unclear. To gain further insights into this mode of filament breakup and to help elucidate the mechanism behind it, we interrogate the evolution in time of both the flow field and the free surface profile just before a capillary wave breakup event occurs. Since it stands to reason to suspect that some sort of interaction is occurring across the symmetry plane $z = 0$, Fig. 4 shows a side-by-side comparison of the results of two simulations involving two filaments, both of Oh = 0.05, albeit with two different initial aspect ratios $L_0 = 22.1$ and 80. To facilitate the comparison, the axial coordinates in Fig. 4 have been shifted such that the bottom ends of both filaments appear stationary at each instant in time. This figure makes plain that initially the dynamics in the two cases are essentially identical as the predominant retraction dynamics are localized to the two ends. This state of affairs persists for quite some time with the retraction being driven by the difference in capillary pressure at the tip and that in the main body of the filament. During this period of time, capillary waves propagate down the lengths of the filaments and, as shown earlier in Fig. 3, the radii at the local minima exhibit sinusoidal oscillatory responses whose magnitudes grow

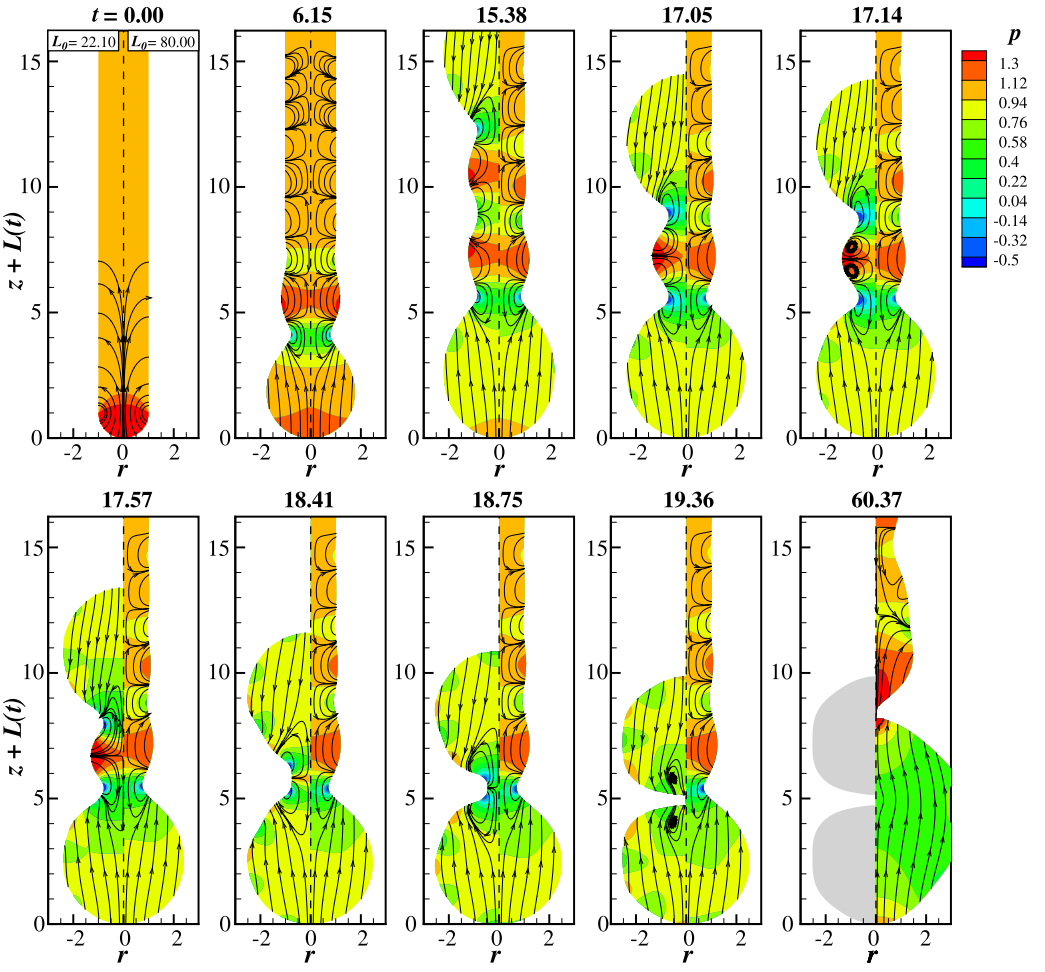

FIG. 4. Evolution in time of the shapes and flow fields—instantaneous streamlines and pressure contours—within two filaments, both of Oh = 0.05 but with different initial aspect ratios of $L_0 = 22.1$ (left) and $L_0 = 80$ (right). The axial coordinate has been shifted by $L(t)$, the distance that the bottom end of a filament has traveled at time t, which has the effect of making the lower end appear stationary in the figure. The difference between the two cases helps to demonstrate the role of the symmetry plane and the interactions across it in the capillary wave breakup mode.

in time but do not yet lead to breakup of the filaments. Later, at time $t = 15.38$, the shorter filament is approaching near full contraction and its two ends are sufficiently close to one another to begin interacting. Here the two local minima, each located where the local filament radius equals R_b on either side of the symmetry plane, just ahead of each receding end, are beginning to tend towards minima in time, signaling that fluid is evacuating out of those regions. Due to symmetry, fluid from the locations of both minima begins draining into the midplane of the filament, leading to a rapid growth of a bulge and buildup of pressure at $z = 0$. This buildup of high pressure causes the flow to reverse in the midplane of the filament, thereby draining fluid away from the middle of the filament. In this case, this drainage is dramatic enough that the out-of-plane curvature of the interface begins to dominate the in-plane curvature and ultimately drives the filament to break. In contrast, at roughly the same time, the ends of the longer filament are still sufficiently far apart that there is negligible interaction across the plane of symmetry to initiate breakup. Indeed, the long filament continues to

retract in much the same way for quite some time and, much later, finally succumbs to end pinching (at time $t = 60.37$).

We will now take advantage of results obtained from simulations of contraction of semi-infinite filaments that succumb to end pinching in furthering our understanding of capillary wave breakup. We recall that end pinching always requires an identical amount of time, and hence also an identical recoil length. These facts formed the basis of the approach used by Hoepffner and Paré [34], who extrapolated results obtained from the recoil of semi-infinite filaments to estimate the critical initial aspect ratio that is required for a retracting filament of finite length to break by end pinching. Since this simple analysis does not apply to capillary wave breakup, they only identified the critical initial aspect ratio at which end pinching will begin to occur and thereby estimated $L_{c,2}$. However, knowing two key facts that are provided by such simulations, we can also readily estimate the values of L_0 for which one might expect to find capillary wave breakup. Namely, we make use of the observation reported in previous paragraphs that capillary wave breakup occurs when a local minimum in the filament's radius is approaching a minimum in time just before the filament fully contracts. By simulating the contraction of a semi-infinite filament, we can determine the instants in time at which R_b is at a minimum for such a filament (cf. Fig. 3), which will also happen to be virtually the same instants in time at which R_b will be at a minimum for all filaments of finite length regardless of the value of L_0. Additionally, we can also estimate the value of the initial aspect ratio that will result in the filament to also be near full contraction at the time when R_b is a minimum. The value of L_0 that is estimated in this manner will be referred to as the predicted initial aspect ratio L_p. The simplest way to estimate L_p is to take the total distance or length contracted (L_{con}) up to this point in time and add to it the length of the blob L_b, which is simply the distance measured from the tip of the filament to the local minimum on the free surface, giving $L_p = L_{\text{con}} + L_b$. The length of the blob is included because it will always be a part of the breakup shape. Performing this analysis on a semi-infinite filament of $\text{Oh} = 0.03$ results in predicted values of $L_p = 7.3$, 14, and 22, all of which are in excellent accord with values obtained from simulations with filaments of finite lengths that are reported in Fig. 2. However, it should be noted that capillary wave breakup may not necessarily occur for values of L_p estimated in this manner if the radius of the minimum has not fallen too far from its initial value of one. Empirical evidence based on a large number of simulations indicates that if R_b has not fallen below approximately 0.7 prior to near full contraction, pinch-off by capillary wave breakup is unlikely to occur.

The analysis presented in the preceding paragraph holds equally well in predicting second capillary wave breakup. However, because capillary waves are viscously damped as they travel down the lengths of filaments, the occurrence of higher-capillary wave breakup events is expected to be less common. Indeed, in some rare circumstances rapid thinning at the third- or a higher-order minimum may result in a third- or higher-order capillary wave breakup. However, the occurrence of such higher-order minima is extremely rare. For example, third-order capillary wave breakup was only observed in one case of a filament of $\text{Oh} = 0.055$ and $L_0 = 72$. Also, only a single case of fourth-order capillary wave breakup was observed and instances of fifth- and higher-order capillary wave breakups were never observed. Cases of third- and higher-order capillary wave breakup are henceforward not considered in this paper. Interestingly, comparison of predicted values of the initial aspect ratio for which first and second capillary wave breakup should occur yield similar values of L_0. Moreover, as the second minimum will reach the symmetry plane before the first minimum, second capillary wave breakup will preempt first capillary wave breakup from arising. Indeed, this is precisely what occurs for the filament of $L_0 = 29$ in Fig. 2. At first glance, this outcome seems counterintuitive since the minima of R_b and R_{b2} are out of phase with respect to each other in time, which is a consequence of their connection to one another via the flow field in that when fluid is draining out of the neighborhood of R_b it is draining into the neighborhood of R_{b2}. However, since they are also separated in space axially, these two factors, when considered together, conspire to give identical initial aspect ratios for which these modes of breakup will appear. Again, due to their connection through the flow fields, if the second minima do not undergo breakup, they will rebound, filling the center with fluid. This in turn means that the

first minima are now draining, which then results in favorable conditions for first capillary wave breakup.

Due to the appearance and disappearance of the capillary wave breakup mode as L_0 is varied at fixed Oh, this intermediate regime has been misrepresented and/or inadequately appreciated in the literature such that earlier studies have entirely missed regions where breakup occurs. For example, the numerical study by Notz and Basaran [29] in general has overestimated the value of $L_{c,1}$ and presented values of the critical initial aspect ratios with large error bars despite being able to accurately model filament contraction. That these authors fell short in this regard was simply due to their inability to properly search the entire phase space spanned by L_0 and Oh because of limitations on computational resources at the time when the work was carried out. Experimental studies [30] have shown evidence of breakup at values of $L_0 < L_{c,2}$ which may be attributable to capillary wave breakup. However, exact replication by simulation of the regions in parameter space where capillary wave breakup occurs in experiments may be difficult since a filament generated in experiments may already have a wavy profile rather than a perfectly cylindrical one at the initial instant when it begins recoiling. Sambath [46] has numerically demonstrated the occurrence of capillary wave breakup in a single case, albeit without realizing that this was indeed the mode of breakup while studying the pinch-off of so-called asymmetric dumbbell filaments in which one of the ends of the filament consists of a superhemispherical cap [6]. More recently, Wang *et al.* [47] have reported instances of capillary wave breakup by studying filament contraction over the range of Ohnesorge numbers $0.003 \leqslant \mathrm{Oh} \leqslant 0.02$.

IV. INVISCID REGIME (Oh < 0.002)

The dynamics of filaments remains virtually unchanged with Oh when the Ohnesorge number lies below a certain value (see, e.g., [29] and the Appendix). Therefore, such nearly inviscid or slightly viscous filaments behave for all practical purposes like inviscid ($\mathrm{Oh} = 0$) filaments. The recoil dynamics is in the inviscid regime when $\mathrm{Oh} < 0.002$. It is now well known that the final mode of breakup in the inviscid regime is end pinching [29]. Filaments that are too short to undergo end pinching are also known to undergo complex oscillations about a sphere of the same volume as the filament [29]. However, such oscillations may result in breakup, giving rise to a wide variety of breakup shapes. If the oscillations do not result in breakup, they eventually die out and the filament comes to rest as a quiescent liquid sphere if Oh is finite or they continue indefinitely if $\mathrm{Oh} = 0$. Thus, the onset of end pinching should determine the value of $L_{c,2}$ in the inviscid regime. Since by definition complex oscillations occur only after full contraction, i.e., when the filament has recoiled so that its aspect ratio has become approximately equal to one, they are not considered when determining the critical initial aspect ratio. Hence, in the case of inviscid filaments, one would expect that $L_{c,1} \equiv L_{c,2}$.

To provide a more thorough analysis of the dynamics in the inviscid regime, the value of the initial aspect ratio is systematically increased from a small value while holding the Ohnesorge number fixed at $\mathrm{Oh} = 0.001$. Figure 5(a) shows a selection of shapes at breakup over a range of L_0 and Fig. 5(b) shows the variation of the breakup time t_b with L_0 obtained from simulations for this value of Oh. While it is readily appreciated that the breakup shapes for $L_0 = 5$, 10, and 15 are identical to those obtained by Notz and Basaran [29] from their simulations, here the results of many other simulations carried out over this parameter range are reported as well. Our simulations show that for values of the initial aspect ratio below $L_0 = 4.5$, filaments will always contract to a sphere, whereas those filaments with L_0 just equal to or a bit larger than 4.5 break after undergoing complex oscillations. As examples, breakup shapes are shown for values of $L_0 = 4.5$ and 5. As L_0 is further increased, the mode of breakup appears to resemble the onset of end pinching for $5.5 < L_0 < 7.6$. Indeed, Notz and Basaran attributed pinch-off and the corresponding breakup shapes in this range to end pinching and thus determined the critical initial aspect ratio to be approximately 5.5. However, if the variation of the breakup time with L_0 is examined over this range of L_0, it is clear that t_b steadily increases with L_0 before this dynamical response is interrupted by another zone of breakup due to

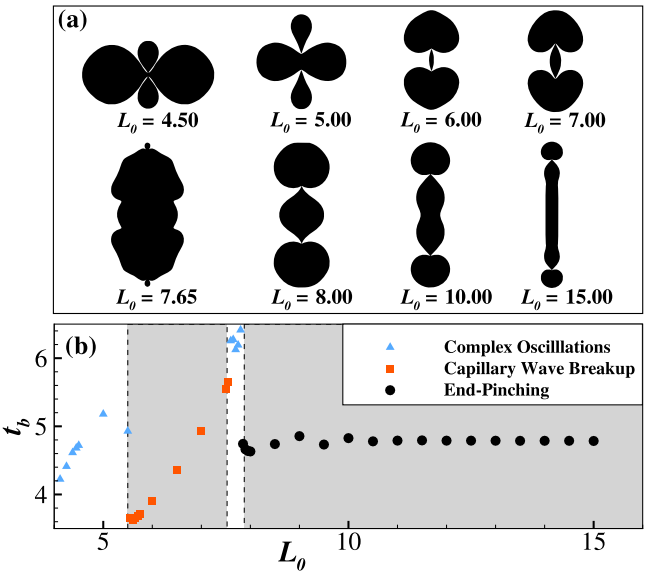

FIG. 5. Breakup shapes and breakup times of filaments of Oh = 0.001. (a) Variation of shapes at breakup (not to scale) with L_0 showing breakup by complex oscillations, capillary wave breakup, and end pinching. (b) Variation of breakup time t_b with L_0. The different types of dynamics that fall into the various categories are identified by triangles, squares, and circles. The regions in gray indicate ones where breakup will occur before full contraction, whereas white regions indicate those where breakup will occur after full contraction and while the filaments are undergoing complex oscillations.

complex oscillations for $7.6 \leqslant L_0 \leqslant 7.85$. The latter zone then gives way to true end pinching as L_0 is further increased; the dynamics become local only to the ends of the filament and the time required for breakup becomes invariant despite further increases in the value of L_0. The aforementioned findings make plain that even for nearly inviscid filaments, $L_{c,1} \neq L_{c,2}$ and in the particular case where Oh = 0.001, $L_{c,1} = 5.53$ whereas $L_{c,2} = 7.83$.

The breakup mode that is referred to in the preceding paragraph that had heretofore been improperly attributed to end pinching in the literature is in fact the first capillary wave breakup mode that was encountered in the discussion of breakup of filaments of intermediate Oh. Therefore, as already stated in the preceding paragraph, even in the case of nearly inviscid filaments the assumption that $L_{c,1} \equiv L_{c,2}$ is invalid. However, the difference in the values of $L_{c,1}$ and $L_{c,2}$ is much smaller for nearly inviscid filaments as compared to filaments of intermediate Oh. Simulations further reveal that for values of $L_0 \gg L_{c,2}$, filaments pinch off droplets repeatedly from their two ends at regular intervals in time and for each breakup event the daughter droplets that are thereby produced are of the same volume.

V. VISCOUS REGIME (Oh > 0.1)

In this section, the fate of highly viscous filaments with Oh > 0.1 is investigated. Simulations show that the contraction dynamics of highly viscous filaments differs from that of intermediately viscous and inviscid filaments in that a neck does not form at the two locations along the free surface where the two receding blobs at each end of the filament connect to its main body. Indeed, it is the formation of these necks that eventually leads to the occurrence of end pinching in less viscous filaments. Since a neck does not form in highly viscous filaments, it was originally thought that filaments in this regime will simply never undergo breakup and will always contract to a sphere. However, as has been shown by Driessen *et al.* [31], the long, slender, and nearly cylindrical

body of such filaments is inherently susceptible to a Rayleigh-Plateau-type instability. Rather than solving the full set of partial differential equations governing the dynamics, these authors solved a simplified one-dimensional approximation to the governing equations when such filaments are subjected to initial perturbations. By comparing the growth rate of the imposed instability to the contraction speed of the filament ends, these authors could then determine the critical initial aspect ratio, which in this case is what is referred to as $L_{c,2}$ in the present paper. The relation predicting the value of $L_{c,2}$ that these authors derived depended on the amplitude of the perturbation as an input.

In order to determine the critical initial aspect ratio that is needed to cause breakup of highly viscous filaments that solely depends on Oh, simulations are performed in which the contraction dynamics of initially unperturbed filaments of extremely long lengths is computationally determined to probe, among other things, if instabilities arise naturally owing to the motion of the two receding ends and lead to filament pinch-off. If one were to consider a quiescent spherical drop or a long fluid cylindrical column, nothing will happen unless the sphere or the cylinder is perturbed. However, a slightly perturbed drop then oscillates and a slightly perturbed column either oscillates or breaks, depending on the wavelength of the imposed perturbation [26]. A filament, of course, is not just a cylindrical column but has two ends which are initially hemispherical caps. As the ends recoil, the resulting motion can provide perturbations to the initially quiescent cylindrical section that can result in the exponential growth of the perturbations and ultimately pinch-off.

The simulations for $\mathrm{Oh} = 0.3$ and ones for larger values of Oh reveal that when the filaments are initially shorter than some critical amount, the two receding ends sweep up fluid as they retract and the growing blobs smoothly merge with the cylindrical section of the filament with no apparent local minima in filament radius at their connection. However, if the filament is long enough, an instability arises along the cylindrical section of the recoiling filament and the destabilization which manifests itself along the entire length of the filament eventually results in nearly simultaneous pinch-off of the filament at a number of locations along its length. Simulations show that when $\mathrm{Oh} = 0.3$ all filaments of $L_0 < 175.5$ contract to spheres while ones of $L_0 > 175.5$ succumb to a Rayleigh-Plateau-type instability. Simulations further reveal that the breakup time t_b, which is the combination of the time that it takes for the instability to grow and ultimately cause pinch-off to occur, is virtually independent of L_0 for all Oh when the Ohnesorge number is sufficiently large, i.e., the curves that show how t_b varies with L_0 are nearly horizontal lines and t_b varies by a few percent as the value of L_0 is varied over a large range, as shown in Fig. 6(a). The critical value of L_0 that is needed to cause filament breakup, however, does increase with Oh, as shown in Fig. 6(b) (see also [48], where it has been shown that inertialess filaments cannot break). Moreover, as a filament's initial aspect ratio is increased above the critical value at a given value of Oh, the filament's length at breakup increases and the number of drops generated from breakup also increases proportionally to the growth of L_0. However, it is further observed that breakup always generates two large drops from the two ends along with a number of smaller, but not necessarily equal, in size droplets. This behavior can be seen in the breakup shapes for $\mathrm{Oh} = 0.3$ shown in Fig. 6(c) for a wide range of initial aspect ratios in excess of $L_{c,2}$.

Simulation of the recoil dynamics of extremely long filaments is computationally costly and direct determination of the critical initial aspect ratio by running a large number of simulations by systematically varying L_0 until there is a change in the dynamics from breakup to no breakup is even more so. However, since the breakup time is relatively constant, or virtually independent of the value of L_0, for a given Oh and because filaments contract at the capillary velocity, which is unity in our nondimensionalization, a single simulation involving a filament of L_0 well in excess of the critical initial aspect ratio can be used to estimate $L_{c,2}$. When using the strategy employed by Hoepffner and Paré [34], the total contraction length at breakup is equated to $L_{c,2}$. Using their methodology to estimate the critical initial aspect ratio for $\mathrm{Oh} = 1$ from a simulation with $L_0 = 450$ yields $L_c \approx 309.4$. Using this estimate, a few targeted simulations can then be performed in its vicinity and it was quickly found that the actual value of L_c is 319.7. The small discrepancy in the estimated and computed values of L_c is due to the fact that at breakup, a filament always has two ends

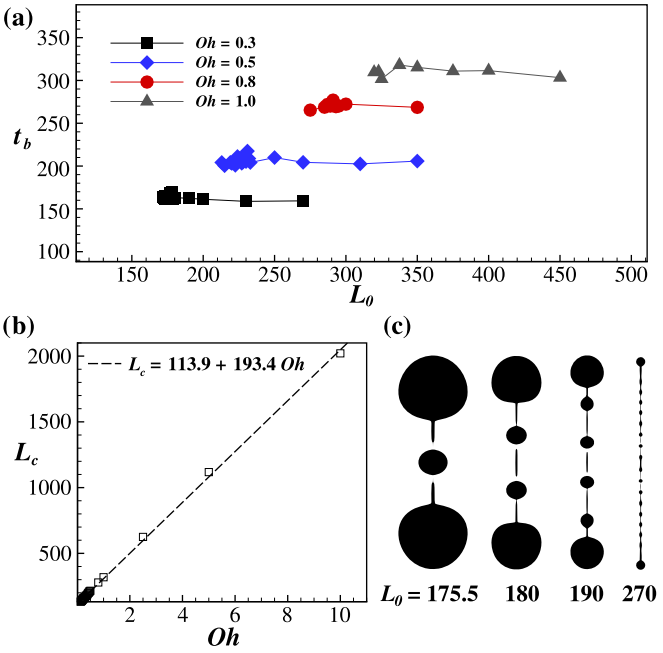

FIG. 6. Breakup time, critical initial aspect ratio, and breakup shapes in the viscous regime. (a) Breakup time t_b as a function of the initial aspect ratio L_0 for several Oh. In each case, $L_{c,1} \approx L_{c,2}$ is the first instance of breakup seen when marching from low to high L_0. (b) Variation of the critical initial aspect ratio L_c [from (a)] with Ohnesorge number Oh. The data points are fit well by the indicated straight line, which shows the linear dependence of L_c on Oh. (c) Variation of breakup shapes at various values of L_0 that are well in excess of $L_{c,2}$ when Oh $= 0.3$.

that are blobs that have swept up fluid during retraction. Since the length of the blob is approximately 12 in this case, adding the blob lengths to the estimated value of the critical breakup length gives an $L_c \approx 321.4$, which is much closer to the actual value determined from simulations. Any additional discrepancy between the estimated and computed values of L_c is due to the interaction of the two halves of the recoiling filament across the symmetry plane $z = 0$. Thus, it has been found that this interaction can either delay or promote breakup even in the viscous regime, albeit to a small extent, similarly to that which occurs in capillary wave breakup in the intermediate regime. However, the influence that the interaction across the plane of symmetry has on the critical aspect ratio in the viscous regime is modest compared to that in the intermediate regime and is especially so given the rather large values of the initial aspect ratio that are needed to cause breakup in the former case compared to the latter one. Thus, in the remainder of the paper, we estimate the values of the critical initial aspect ratio in the viscous regime as described above assuming $L_{c,1} \approx L_{c,2}$.

The approach described above for estimating L_c was carried out over the range of Ohnesorge numbers $0.1 <$ Oh $\leqslant 10$ and the estimated critical initial aspect ratio L_c was found to vary linearly with Oh. The linearity of the dependence of the critical aspect ratio upon the Ohnesorge number can be explained through a simple comparison of the timescales involved in the problem, namely, those of filament contraction and filament breakup. As has already been stated earlier, the filament contracts at the capillary velocity. Thus, in dimensional form, the capillary velocity is given by $v_{\text{cap}} = \sqrt{\gamma/\rho\tilde{R}}$ and therefore the time for contraction is $t_{\text{con}} = \tilde{L}_0/v_{\text{cap}} = \tilde{L}_0\sqrt{\rho\tilde{R}/\gamma}$. For highly viscous filaments, the breakup time should scale with the viscocapillary time $t_{\text{visc}} = \mu\tilde{R}/\gamma$ [49]. Equating the two timescales, we find that the dimensional value of the critical initial aspect ratio should vary as $\tilde{L}_c \sim \mu\sqrt{\tilde{R}/\rho\gamma}$ or its dimensionless counterpart $L_c \equiv \tilde{L}_c/\tilde{R}$ should scale as $L_c \sim$ Oh.

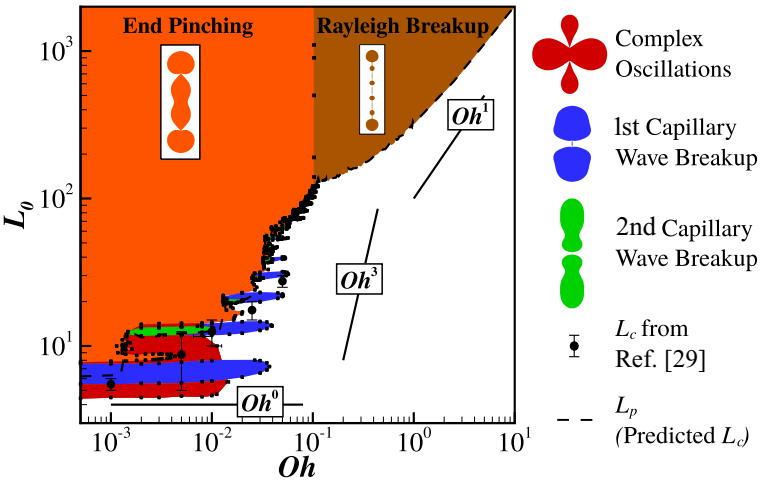

FIG. 7. Phase diagram in the space of L_0 and Oh summarizing the fate of contracting Newtonian filaments that has been obtained after performing over 3000 simulations. Error bars, or uncertainties, on the boundaries between different breakup modes are shown in the figure but are typically too small to be visible. In the phase diagram, estimates of the critical initial aspect ratio obtained in the study of Notz and Basaran [29] are also shown as well as the simple scaling predictions obtained by comparing the contraction time to the relevant timescale of breakup in the three regimes (inviscid, intermediate, and viscous).

VI. CONCLUSION

By means of an exhaustive computational study involving more than 3000 simulations, the entire parameter space comprised of the initial aspect ratio L_0 and Ohnesorge number Oh governing the dynamics of recoil of Newtonian filaments has been explored, and a different breakup mode, capillary wave breakup, has been discovered. Although capillary wave breakup mode has been found to occur for all filaments of Oh < 0.1, it is more prevalent in the intermediate range of Oh rather than the nearly inviscid range where filaments are more likely to succumb to end pinching. The occurrence of this mode of breakup is highly dependent on the initial aspect ratio L_0, and it has been found to differ from all other breakup modes in that it only occurs at discrete intervals of L_0 for a given Oh, which in turn causes a large separation in the values of $L_{c,1}$ and $L_{c,2}$ at intermediate values of Oh. One main consequence of this large separation in the two critical initial aspect ratios is that care should be exercised when comparing values of the critical initial aspect ratio from different sources found in literature. For example, whereas Notz and Basaran [29] have determined and report what is called $L_{c,1}$ in this paper, studies such as those carried out by Driessen *et al.* [31] and Hoepffner and Paré [34] have predicted and report the critical initial aspect ratio referred to as $L_{c,2}$ in this paper. Furthermore, it is worth noting that in experiments, occurrence of capillary wave breakup may easily be missed and the ranges of parameter values where it may occur could shift, depending on the initial conditions imposed on the filament as it begins to contract (discussed below).

Using this understanding as to when capillary breakup may occur, the aforementioned parametric study was used to generate a phase or operability diagram summarizing the fate of Newtonian filaments in the space spanned by L_0 and Oh which is presented as a log-log plot in Fig. 7. Although there are many salient features to this phase diagram, one pertains to the general nature in which the critical initial aspect ratio increases with Oh. In the preceding section, the retraction time of a filament was balanced with the characteristic time for breakup in the viscous regime to deduce that there was a linear dependence of the critical initial aspect ratio on the Ohnesorge number. Repeating that analysis using either the inertial-capillary timescale $t_{\text{cap}} = \sqrt{\rho \tilde{R}^3/\gamma}$ or the inertial-viscous

timescale $t_{IV} = \mu^3/\rho\gamma^2$ as the characteristic timescales for breakup in the inviscid and intermediate regimes [49], respectively, predicts no dependence of L_c on Oh in the inviscid regime and $L_c \sim \mathrm{Oh}^3$ in the intermediate regime. In Fig. 7, lines of slopes of 0, 3, and 1 are plotted corresponding to these simple scaling laws in all three regimes. The simple scaling laws capture well the overall trends shown in the phase diagram in the inviscid and the viscous regimes. However, in the intermediate regime, an exponent between 1 and 3 rather than the value of exactly 3 obtained from the simple scaling argument appears to describe the overall variation of the critical initial aspect ratio with Ohnesorge number. That the simple-minded scaling argument falls short in the intermediate regime should not be all that surprising given the complexity and the fine-grained nature of the actual breakup dynamics in that regime, including the steplike or stairlike response due to the discrete nature of the capillary wave breakup mode.

Furthermore, another interesting aspect of the phase diagram is that in nearly all instances of first capillary wave breakup, there is a smaller subset of second capillary wave breakup located within the same region on the phase diagram, which is expected since both modes of breakup were predicted to occur in the same range of L_0 for a given Oh. The only exception is seen in the first interval of capillary wave breakup from about $5.5 < L_0 < 7.6$ and is simply due to the fact that the filament is so short in these cases that there is no time for the capillary wave to form a substantial second minimum before it reaches the midplane of the filament. Remarkably, and as has already been stated in Sec. III, instances of the third and the fourth capillary have also been observed but are so rare that they are not shown in the phase diagram depicted in Fig. 7.

The high-accuracy simulation results reported in this paper that are made possible by the use of a sharp interface method and the deployment of highly adaptive meshes [17,29,50–53] can be applied to other situations where analysis of the contraction dynamics of filaments is important. Among such problems, especially noteworthy are contraction dynamics where filaments are covered with surfactants [53–55] and also situations where charged and/or uncharged filaments recoil in the presence of electric fields [41]. Also of great interest in computational studies of contraction dynamics of both simple filaments of Newtonian fluids with clean interfaces as in this paper and more complex filaments referred to in the preceding sentence is the matter of initial conditions. In this paper, the filament initially has the profile of a cylinder that is terminated at both ends by identical hemispherical caps having the same radii as the cylinder, i.e., a so-called symmetric filament, and the fluid within it is quiescent. Also of interest is the dynamics of filaments with more complex initial profiles. Of particular interest are asymmetric filaments which resemble satellite droplets formed during dripping and jetting from nozzles [1,36] and have initial profiles that resemble baseball bats or cones whose tips have been removed and both ends of which have been capped by two sections of spheres of unequal radii [17]. Equally interesting is the dynamics of so-called dumbbell filaments which resemble inkjet drops [16] and whose initial profiles consist of a cylindrical body that is capped at both ends by spheres of unequal radii [6,46]. Moreover, at the initial instant, the surfaces of the filaments may have corrugations to better mimic ligaments or filaments formed during experiments on atomization and spraying [20,56]. Furthermore, imposing initial conditions of a quiescent filament may not always be appropriate when using simulations to model experiments. Thus, consideration of different realistic initial velocity profiles within contracting filaments (see, e.g., [46]) would constitute yet another worthy avenue of future research in the field.

APPENDIX: ACCURACY CHECKS—MESH INDEPENDENCE AND VALIDATION OF NUMERICAL RESULTS

In this Appendix, the results of a number of accuracy checks and validation studies are shown. These have been carried out to ensure the accuracy of the algorithm and the simulations used to generate the results that are presented in the main text. In particular, in obtaining the results reported in this paper, mesh or grid independence studies were carried out in different regions of the

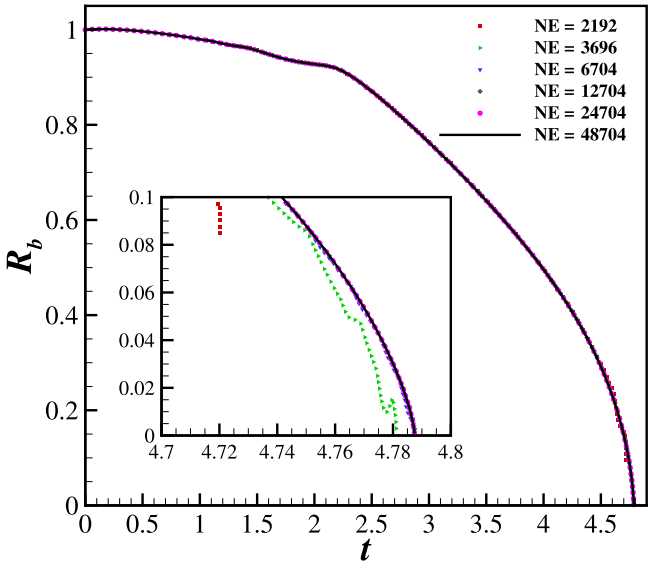

FIG. 8. Variation of the first minimum in filament radius R_b with time t: comparison of computational predictions obtained with six different meshes. The total number of elements (NE) is successively (roughly) doubled, while the number of (nonuniform) elements in the radial direction is held fixed at 16. Solutions obtained using meshes with 6074 to 48 704 elements yield nearly identical results and the mesh chosen in the body of the paper corresponds to that with 12 704 elements. The inset shows the computed solutions near breakup and helps highlight the inadequacy of the coarsest two meshes. Here Oh $= 10^{-3}$ and $L_0 = 15$.

parameter space before mining or exploring in detail the dynamics of filament contraction in those regions.

First, mesh independence of solutions is demonstrated in the intermediate- to low-Ohnesorge-number range of the phase space studied in this paper. Accurately predicting the dynamics of contracting filaments at small values of the Ohnesorge number is typically most challenging owing to the overturning of the free surface that results in extreme mesh deformations as breakup is approached [29]. Therefore, the results of a mesh independence study are first presented for the situation in which Oh $= 10^{-3}$ and $L_0 = 15$. A similar grid refinement study has been carried out by Notz and Basaran [29], who used elliptic mesh generation as in this paper but also successfully benchmarked their simulation results against ones obtained with an algorithm that employed a spine parametrization of the free surface and the underlying mesh. Since many types of grid refinement studies can be carried out as also summarized in Ref. [29], we will describe the results of one such study. Figure 8 shows the variation of the first minimum in filament radius R_b with time t in six different cases in which the number of elements in the mesh has been successively doubled from one case to the next. In this particular example, 16 nonuniform elements are used in the radial direction, but the total number of elements has been increased by the addition of axial elements to the mesh.

Figure 8 shows that the simulations using 2192 and 3696 elements exhibit a clear departure from the ones using more dense or refined meshes, with the highly coarse mesh of 2192 elements even failing to reach the breakup criterion of the minimum neck radius reaching $R_{\min} = 10^{-3}$. A close inspection of the meshes near breakup reveals that in both cases, the mesh densities are insufficient to capture the overturning of the interface at this small value of Oh resulting in highly deformed, jagged interfaces. Reassuringly, the other four cases using larger numbers of elements give rise to nearly identical dynamical responses during the entirety of the simulations with the case of 6704 elements exhibiting a barely visible difference from the other three cases with the denser meshes.

TABLE I. Percentage difference in breakup time t_b obtained with a mesh using the indicated number of elements relative to a fine mesh composed of 48 704 elements. Here Oh = 0.1 and $L_0 = 150$.

Total number of elements	% difference in t_b
6704	0.39%
12704	0.09%
23504	0.20%

The breakup time obtained with the third densest mesh of 12 704 elements differs by as little as 0.0014% from the breakup time of 4.787 obtained with the densest mesh. It is also reassuring that for this set of parameter values, the breakup time obtained in this work is identical to that obtained by Notz and Basaran [29] with their most refined meshes. Also, results of additional mesh refinement studies have shown that the number of axial elements needed to yield mesh-independent results scaled linearly with L_0 in that doubling the value of L_0 required doubling the number of elements.

In addition to the nearly inviscid case that has just been discussed, the results of a mesh independence study are presented next for two cases of higher Oh: One of these, for a filament of Oh = 0.1 and $L_0 = 150$, lies near the boundary between the intermediate and viscous regimes and the other, for a filament of Oh = 0.2 and $L_0 = 250$, squarely falls in the viscous regime. In both cases, the mesh density was again progressively doubled by varying the number of axial elements while holding the number of radial elements constant at 16. The results of this investigation are summarized in Tables I and II, where the percentage difference in the breakup time from the most dense case is shown for each of the less dense meshes used. In the case of the filament of Oh = 0.1, the dynamics of which lies in the part of the intermediate regime that will give way to the viscous regime if Oh were to be increased slightly, the contracting filament is expected to succumb to end pinching after many successive escapes from pinch-off given the filament's long length. Indeed, the results of Table I make plain that even including the simulation with the coarsest mesh shown in the table, the computed results are independent of the number of elements used as the breakup time determined with any of the less dense meshes used differs by a small fraction of a percent from the mesh with the largest number of elements. Moreover, the simulations show that regardless of the mesh density used, the dynamics computed with all of the meshes experiences the same number of escapes before finally succumbing to pinch-off by end pinching. In the case of the filament of Oh = 0.2, the dynamics of which lies squarely in the viscous regime, the recoiling filament is expected to ultimately succumb to a Rayleigh-Plateau-like instability. In this case, given the larger value of the initial aspect ratio compared to the previous case, the densest mesh contains about twice as many elements as the earlier one. As shown in Table II, the percentage error in breakup

TABLE II. Percentage difference in breakup time t_b obtained with a mesh using the indicated number of elements relative to a fine mesh composed of 80 704 elements. Here Oh = 0.2 and $L_0 = 250$.

Total number of elements	% difference in t_b
12704	3.50%
20704	2.42%
40704	0.48%

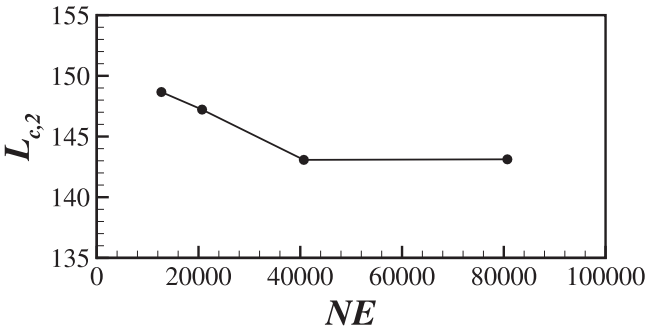

FIG. 9. Variation of the computationally predicted critical initial aspect ratio $L_{c,2}$ with the number of elements in the mesh when Oh = 0.2. The results show that the computed value of $L_{c,2}$ converges as the mesh density is systematically increased.

time with the coarsest mesh is about 3.5% but rapidly decreases as the mesh density is successively doubled. Furthermore, the computationally predicted value of the critical initial aspect ratio $L_{c,2}$ when Oh = 0.2 converges with systematic mesh refinement or is invariant to further increases in the number of elements, as shown in Fig. 9. Therefore, given the findings summarized above, meshes with 23 504 elements and 40 704 elements have been used to obtain solutions for viscous filaments of Oh = 0.1 and Oh = 0.2 shown in the main text.

Next, the results of a study are presented to demonstrate how small the Ohnesorge number has to be for the dynamics to lie in the inviscid limit (Oh $\rightarrow$ 0). Vorticity is generated at a free surface such as the surface of a recoiling filament because of flow past regions of surface curvature [57]. Therefore, the free surface flow that arises during filament recoil is not an irrotational or a potential flow no matter how small the Ohnesorge number and some surprising phenomena may arise at low Oh. Indeed, the role of vorticity dynamics and unsteady boundary layer separation has already been demonstrated in the work of Song and Tryggvason [58], who studied the recoil of liquid sheets which is the two-dimensional analog of the three-dimensional but axisymmetric filament recoil problem analyzed in the present paper, and subsequently by Hoepffner and Paré [34], who studied the breakup of contracting filaments as in this paper. In Sec. IV, the boundary between the intermediate and the inviscid regimes is stated to be roughly around Oh = 2×10^{-3}. Therefore, a series of simulations has been carried out in which the value of Oh has been roughly halved in a systematic manner starting at Oh = 2×10^{-3} and ending at Oh = 10^{-4} as shown in Fig. 10. The results show that the curves depicting the variation in time of R_b at early times essentially lie on top of each other before deviations in behavior can be observed between the case with the highest Ohnesorge number and the others as breakup is approached. Specifically, the case with the largest value of Oh = 2×10^{-3} experiences an escape from end pinching as described by Hoepffner and Paré [34], a response which is characteristic of the intermediate regime, whereas all the other cases experience immediate end pinching, a response which is characteristic of the inviscid regime. As shown by Hoepffner and Paré [34], in the intermediate regime, a vortex ring forms at the neck of the recoiling filament and detaches from the free surface. Subsequently, flow from the blob toward the neck causes the neck to reopen and the filament escapes end pinching. Furthermore, as Oh is systematically decreased, the curves of R_b versus t for different values of Oh near breakup also begin to collapse onto a single master curve. Indeed, the difference in the breakup time when Oh is decreased by an order of magnitude from 10^{-3} to 10^{-4} is only 1.8%, whereas the corresponding difference in the value of the aspect ratio at breakup is less than 1%. Moreover, when the value of the Ohnesorge number is halved from 2×10^{-4} to 10^{-4}, the breakup time changes by about 0.15%, indicating that the limit of Oh = 0 has been reached. The small differences in breakup times and aspect ratios, and the indistinguishable shapes at breakup, of filaments of Oh = 10^{-3} and those of Oh $\rightarrow$ 0, justifies why filaments of Oh = 10^{-3} are referred to as inviscid or nearly inviscid filaments.

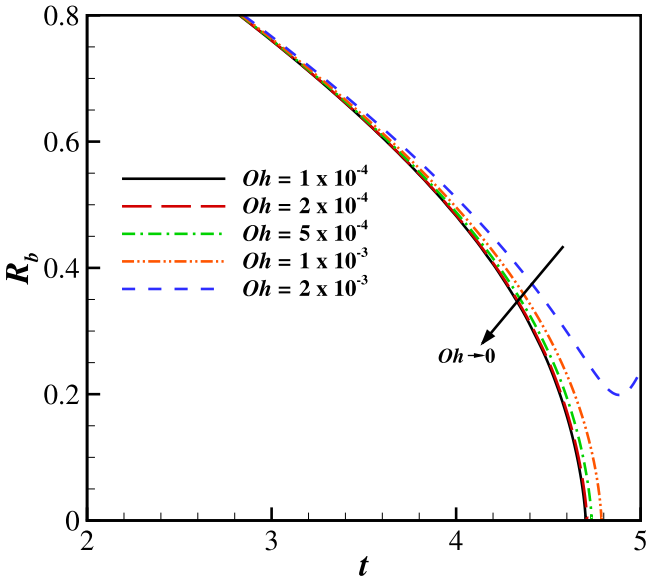

FIG. 10. Approach to the inviscid limit: variation of the first minimum in filament radius R_b with time t for filaments of different Oh. Here the value of the Ohnesorge number is successively (roughly) halved from 2×10^{-3} to 10^{-4}. The filament with the largest value of Oh experiences an escape from end pinching. All the other filaments of smaller Oh immediately end pinch and the curves of R_b versus t for each case collapse onto a single curve as Oh is progressively decreased. Here $L_0 = 15$.

Predictions made with algorithms and/or codes used for solving free surface flows with breakup or coalescence, as in breakup or pinch-off as in this paper, must accord with well known scaling laws that describe the dynamics near appropriate space-time singularities [18]. Demonstration that an algorithm or code can correctly predict scaling exponents and sometimes also prefactors in theoretical scaling laws provides a test that is much more stringent than that possible from experiments [50,51,53]. Since the dynamics near the space-time singularity is universal, it is immaterial whether this demonstration is made in the context of breakup during filament recoil (see, e.g., [29]) or some other free surface flow involving pinch-off. Here we will demonstrate the capabilities of the algorithm or code of this paper in this regard by using it to simulate capillary pinching of liquid jets or columns as in one of the pioneering studies in the field [50]. Thus, the algorithm or code used here was adapted to simulate the breakup of an indefinitely long jet of an incompressible Newtonian fluid that is surrounded by a dynamically passive fluid, i.e., the liquid filament of this paper is merely replaced by a liquid column or jet. In these simulations, we subject an initially quiescent jet to an infinitesimal-amplitude, axially periodic perturbation of dimensionless wavelength (made dimensionless with the undisturbed radius of the jet) of 20 (because of universality, the actual wavelength is immaterial so long as it is sufficiently long to cause instability). For purposes of illustration, we consider the dynamics of capillary thinning and breakup for the situation in which the Ohnesorge number equals 0.1 (Oh is defined in the same manner as before except $\tilde{R}$ now stands for the dimensional radius of the unperturbed jet rather than that of the filament). We then monitor the variation of the dimensionless minimum radius of the jet $R_{\min}$ (made dimensionless with $\tilde{R}$) with time remaining until pinch-off, $\tau \equiv t_b - t$, where t_b is the breakup time. It is known from theory that the final scaling regime in capillary pinch-off is the inertial-viscous regime [18] regardless of Oh, but that during thinning the scaling response may pass through intermediate inviscid and viscous regimes depending on the value of Oh before attaining the final inertial-viscous regime as τ and/or $R_{\min} \to 0$ [50]. When Oh $= 0.1$, the jet is expected to pass through all three regimes as it tends toward pinch-off [50,51].

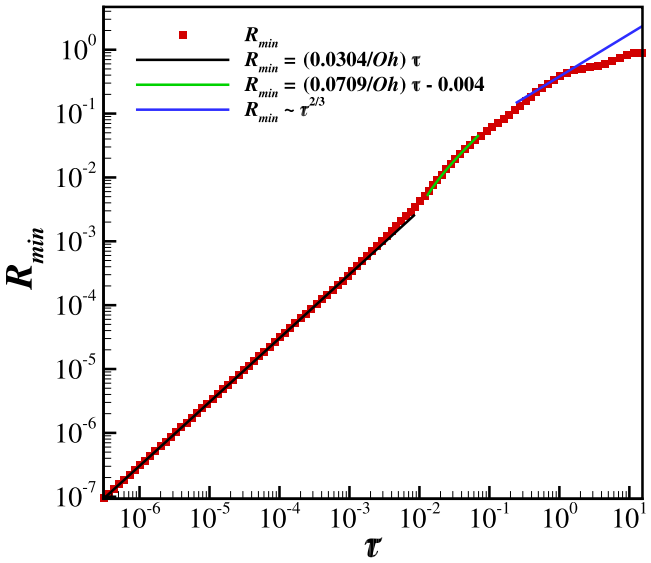

FIG. 11. Variation of $R_{\min}$ with τ during capillary thinning of a jet of Oh $= 0.1$ that is subjected to an initial perturbation of infinitesimal amplitude and dimensionless axial wavelength of 20. Red squares show data points obtained from simulations. Black, green, and purple curves show the scaling law for the final inertial-viscous regime, the scaling law for the intermediate viscous regime, and the scaling law for the initial inviscid scaling regime (see the text).

In Fig. 11, the variation of $R_{\min}$ with τ is shown from the onset of the dynamics, when the dimensionless minimum radius of the jet is of order one ($R_{\min} \approx 1$) until the minimum radius has fallen by seven orders of magnitude ($R_{\min} \approx 10^{-7}$). The results show that as expected, once the initial transients have died out, the thinning lies in the inviscid regime where $R_{\min} \sim \tau^{2/3}$ [59,60], then it gives way to the viscous regime where $R_{\min} \sim \tau$ with a prefactor of 0.0709/Oh [61], and ultimately the dynamics transitions into the asymptotic or final inertial-viscous regime where $R_{\min} \sim \tau$ with a prefactor of 0.0304/Oh [62] (see [18,50] for a summary of the various scaling regimes). The computational results shown exhibit excellent agreement with theory down to a small value of $R_{\min} = 10^{-7}$, a value that is orders of magnitude smaller than that reported when using a multidimensional free surface flow algorithm or code to solve the Navier-Stokes equations with inertia to probe the dynamics near a pinch-off singularity (it is noteworthy that the value of $R_{\min}$ achieved here is 3–4 orders of magnitude smaller than that realized in Refs. [50,51]). The results shown in Fig. 11 were achieved using a higher mesh density than that which is needed for the analysis of filament recoil reported in this paper in conjunction with an adaptive *h*-refinement technique first demonstrated by Anthony and Basaran [63,64]. Although such super-refined meshes and the *h*-refinement technique were used to confirm and lend further credence to the accuracy of the computational results reported in this paper and/or speed up the computations compared to ones where a very fine mesh, albeit with a fixed number of elements, is used throughout the simulations, mesh-independent results reported here on the dynamics of filament contraction, viz., dynamical regimes, breakup shapes, and breakup times, could be obtained without the use of these advanced techniques and without having to reach such low values of $R_{\min}$.

[1] B. Ambravaneswaran, E. D. Wilkes, and O. A. Basaran, Drop formation from a capillary tube: Comparison of one-dimensional and two-dimensional analyses and occurrence of satellite drops, Phys. Fluids **14**, 2606 (2002).

[2] H. P. Le, Progress and trends in ink-jet printing technology, J. Imaging Sci. Technol. **42**, 49 (1998).
[3] O. A. Basaran, H. Gao, and P. P. Bhat, Nonstandard inkjets, Annu. Rev. Fluid Mech. **45**, 85 (2013).
[4] J. R. Castrejón-Pita, K. J. Kubiak, A. A. Castrejón-Pita, M. C. T. Wilson, and I. M. Hutchings, Mixing and internal dynamics of droplets impacting and coalescing on a solid surface, Phys. Rev. E **88**, 023023 (2013).
[5] H. Wijshoff, The dynamics of the piezo inkjet printhead operation, Phys. Rep. **491**, 77 (2010).
[6] S. D. Hoath, S. Jung, and I. M. Hutchings, A simple criterion for filament break-up in drop-on-demand inkjet printing, Phys. Fluids **25**, 021701 (2013).
[7] M. S. Gebhard and L. E. Scriven, Reduction of air bubbles in spray-applied coatings, J. Coat. Technol. **66**, 27 (1994).
[8] A. Altieri, S. A. Cryer, and L. Acharya, Mechanisms, experiment, and theory of liquid sheet breakup and drop size from agricultural nozzles, Atomization Sprays **24**, 695 (2014).
[9] B. Keshavarz, V. Sharma, E. C. Houze, M. R. Koerner, J. R. Moore, P. M. Cotts, P. Threlfall-Holmes, and G. H. Mckinley, Studying the effects of elongational properties on atomization of weakly viscoelastic solutions using Rayleigh Ohnesorge jetting extensional rheometry (ROJER), J. Non-Newtonian Fluid Mech. **222**, 171 (2015).
[10] P. Calvert, Printing cells, Science **318**, 208 (2007).
[11] M. Guvendiren, J. Molde, R. Soares, and J. Kohn, Designing biomaterials for 3D printing, ACS Biomater. Sci. Eng. **2**, 1679 (2016).
[12] R. D. Boehm, P. R. Miller, J. Daniels, S. Stafslien, and R. J. Narayan, Inkjet printing for pharmaceutical applications, Mater. Today **17**, 247 (2014).
[13] B. Derby, Inkjet printing of functional and structural materials: Fluid property requirements, feature stability, and resolution, Annu. Rev. Mater. Res. **40**, 395 (2010).
[14] A. Teichler, J. Perelaer, and U. S. Schubert, Inkjet printing of organic electronics comparison of deposition techniques and state-of-the-art developments, J. Mater. Chem. C **1**, 1910 (2013).
[15] P. Sarobol, A. Cook, P. G. Clem, D. Keicher, D. Hirschfeld, A. C. Hall, and N. S. Bell, Additive manufacturing of hybrid circuits, Annu. Rev. Mater. Res. **46**, 41 (2016).
[16] J. Eggers and E. Villermaux, Physics of liquid jets, Rep. Prog. Phys. **71**, 036601 (2008).
[17] P. K. Notz, A. U. Chen, and O. A. Basaran, Satellite drops: Unexpected dynamics and change of scaling during pinch-off, Phys. Fluids **13**, 549 (2001).
[18] J. Eggers, Nonlinear dynamics and breakup of free-surface flows, Rev. Mod. Phys. **69**, 865 (1997).
[19] E. Villermaux, Fragmentation, Annu. Rev. Fluid Mech. **39**, 419 (2007).
[20] Y. Wang, K. S. Im, and K. Fezzaa, Similarity between the Primary and Secondary Air-Assisted Liquid Jet Breakup Mechanism, Phys. Rev. Lett. **100**, 154502 (2008).
[21] G. I. Taylor, The dynamics of thin sheets of fluid. III. Disintegration of fluid sheets, Proc. R. Soc. London Ser. A **253**, 313 (1959).
[22] A. L. Altieri and S. A. Cryer, Break-up of sprayed emulsions from flat-fan nozzles using a hole kinematics model, Biosyst. Eng. **169**, 104 (2018).
[23] H. A. Stone, B. J. Bentley, and L. G. Leal, An experimental study of transient effects in the breakup of viscous drops, J. Fluid Mech. **173**, 131 (1986).
[24] H. A. Stone, Dynamics of drop deformation and breakup in viscous fluids, Annu. Rev. Fluid Mech. **26**, 65 (1994).
[25] J. A. F. Plateau, *Statique Experimentale et Theorique des Liquides Soumis aux Seules Forces Moleculaires: Tome Premier* (Gauthier-Villars, Paris, 1873).
[26] Lord Rayleigh, On the stability, or instability, of certain fluid motions, Proc. London Math. Soc. **s1-11**, 57 (1879).
[27] D. H. Michael, Meniscus stability, Annu. Rev. Fluid Mech. **13**, 189 (1981).
[28] R. M. S. M. Schulkes, The contraction of liquid filaments, J. Fluid Mech. **309**, 277 (1996).
[29] P. K. Notz and O. A. Basaran, Dynamics and breakup of a contracting liquid filament, J. Fluid Mech. **512**, 223 (2004).
[30] A. A. Castrejón-Pita, J. R. Castrejón-Pita, and I. M. Hutchings, Breakup of Liquid Filaments, Phys. Rev. Lett. **108**, 074506 (2012).

[31] T. Driessen, R. Jeurissen, H. Wijshoff, F. Toschi, and D. Lohse, Stability of viscous long liquid filaments, Phys. Fluids **25**, 062109 (2013).
[32] J. Eggers and T. F. Dupont, Drop formation in a one-dimensional approximation of the Navier-Stokes equation, J. Fluid Mech. **262**, 205 (1994).
[33] H. J. Subramani, H. K. Yeoh, R. Suryo, Q. Xu, B. Ambravaneswaran, and O. A. Basaran, Simplicity and complexity in a dripping faucet, Phys. Fluids **18**, 032106 (2006).
[34] J. Hoepffner and G. Paré, Recoil of a liquid filament: Escape from pinch-off through creation of a vortex ring, J. Fluid Mech. **734**, 183 (2013).
[35] J. Q. Feng and O. A. Basaran, Shear flow over a translationally symmetric cylindrical bubble pinned on a slot in a plane wall, J. Fluid Mech. **275**, 351 (1994).
[36] E. D. Wilkes, S. D. Phillips, and O. A. Basaran, Computational and experimental analysis of dynamics of drop formation, Phys. Fluids **11**, 3577 (1999).
[37] K. N. Christodoulou and L. E. Scriven, Discretization of free surface flows and other moving boundary problems, J. Comput. Phys. **99**, 39 (1992).
[38] Y. C. Liao, O. A. Basaran, and E. I. Franses, Effects of dynamic surface tension and fluid flow on the oscillations of a supported bubble, Colloids Surf. A **282–283**, 183 (2006).
[39] P. P. Bhat, O. A. Basaran, and M. Pasquali, Dynamics of viscoelastic liquid filaments: Low capillary number flows, J. Non-Newtonian Fluid Mech. **150**, 211 (2008).
[40] J. D. Paulsen, J. C. Burton, S. R. Nagel, S. Appathuri, M. T. Harris, and O. A. Basaran, The inexorable resistance of inertia determines the initial regime of drop coalescence, Proc. Natl. Acad. Sci. USA **109**, 6857 (2012).
[41] R. T. Collins, K. Sambath, M. T. Harris, and O. A. Basaran, Universal scaling laws for the disintegration of electrified drops, Proc. Natl. Acad. Sci. USA **110**, 4905 (2013).
[42] P. M. Gresho and R. L. Sani, *Incompressible Flow and the Finite Element Method* (Wiley, New York, 2000).
[43] P. Hood, Frontal solution program for unsymmetric matrices, Int. J. Numer. Methods Eng. **10**, 379 (1976).
[44] C. R. Anthony, Dynamics of retracting films and filaments near singularities, Ph.D. thesis, Purdue University, 2017.
[45] O. A. Basaran, Nonlinear oscillations of viscous liquid drops, J. Fluid Mech. **241**, 169 (1992).
[46] K. Sambath, Dynamics of drop disintegration and coalescence with and without electric fields, Ph.D. thesis, Purdue University, 2013.
[47] F. Wang, F. Contó, N. Naz, J. R. Castrejón-Pita, A. A. Castrejón-Pita, C. Bailey, W. Wang, J. Feng, and Y. Sui, A fate-alternating transitional regime in contracting liquid filaments, J. Fluid Mech. **860**, 640 (2018).
[48] J. Eggers and M. A. Fontelos, Isolated inertialess drops cannot break up, J. Fluid Mech. **530**, 177 (2005).
[49] B. Ambravaneswaran, H. J. Subramani, S. D. Phillips, and O. A. Basaran, Dripping-Jetting Transitions in a Dripping Faucet, Phys. Rev. Lett. **93**, 034501 (2004).
[50] J. R. Castrejón-Pita, A. A. Castrejón-Pita, S. S. Thete, K. Sambath, I. M. Hutchings, J. Hinch, J. R. Lister, and O. A Basaran, Plethora of transitions during breakup of liquid filaments, Proc. Natl. Acad. Sci. USA **112**, 4582 (2015).
[51] Y. Li and J. E. Sprittles, Capillary breakup of a liquid bridge: Identifying regimes and transitions, J. Fluid Mech. **797**, 29 (2016).
[52] C. R. Anthony, P. M. Kamat, S. S. Thete, J. P. Munro, J. R. Lister, M. T. Harris, and O. A. Basaran, Scaling laws and dynamics of bubble coalescence, Phys. Rev. Fluids **2**, 083601 (2017).
[53] P. M. Kamat, B. W. Wagoner, S. S. Thete, and O. A. Basaran, Role of Marangoni stress during breakup of surfactant-covered liquid threads: Reduced rates of thinning and microthread cascades, Phys. Rev. Fluids **3**, 043602 (2018).
[54] Y. C. Liao, E. I. Franses, and O. A. Basaran, Deformation and breakup of a stretching liquid bridge covered with an insoluble surfactant monolayer, Phys. Fluids **18**, 022101 (2006).
[55] P. M. Kamat, A study of singularities in drops and bubbles under the Influence of non-Newtonian surface and bulk rheology, Ph.D. thesis, Purdue University, 2017.
[56] E. Villermaux, P. Marmottant, and J. Duplat, Ligament-Mediated Spray Formation, Phys. Rev. Lett. **92**, 074501 (2004).

[57] T. Lundgren and P. Koumoutsakos, On the generation of vorticity at a free surface, J. Fluid Mech. **382**, 351 (1999).
[58] M. Song and G. Tryggvason, The formation of thick borders on an initially stationary fluid sheet, Phys. Fluids **11**, 2487 (1999).
[59] Y.-J. Chen and P. H. Steen, Dynamics of inviscid capillary breakup: Collapse and pinchoff of a film bridge, J. Fluid Mech. **341**, 245 (1997).
[60] R. F. Day, E. J. Hinch, and J. R. Lister, Self-Similar Capillary Pinchoff of an Inviscid Fluid, Phys. Rev. Lett. **80**, 704 (1998).
[61] D. T. Papageorgiou, On the breakup of viscous liquid threads, Phys. Fluids **7**, 1529 (1995).
[62] J. Eggers, Universal Pinching of 3D Axisymmetric Free-Surface Flow, Phys. Rev. Lett. **71**, 3458 (1993).
[63] C. R. Anthony and O. A. Basaran, 71st Annual Meeting of the APS Division of Fluid Dynamics, Atlanta, 2018 [Bull. Am. Phys. Soc. 63, Q05.00009 (2018)].
[64] C. R. Anthony and O. A. Basaran, *20th International Symposium on Finite Element Methods in Flow Problems, Chicago, 2019* (IACM, Barcelona, 2019).